Trans. JWRI, Vol. 23 (1994), No. 2

# Role of Secondary Austenite on Corrosion and Stress Corrosion Cracking of Sensitized Duplex Stainless Steel Weldments†

**Toshio KURODA* and Fukuhisa MATSUDA****

**Abstract**

*The role of secondary austenite on corrosion and stress corrosion cracking in high temperature water for sensitized duplex stainless steel weldment was investigated using transmission electron microscopy and fractography.*

*Pitting potential measurements, 10% oxalic acid tests (ASTM A262A), Strauss tests (ASTM A262E) and Huey tests (ASTM A262C) were carried out for the corrosion assessment. For stress corrosion cracking, the slow strain rate testing (SSRT) was carried out at 562K with 8 ppm dissolved oxygen under 8 MPa at a strain rate of $4.17x10^{-6}s^{-1}$.*

*Volume fraction of γphase decreased with increasing peak temperature and the grain size of the γphase increased with increasing peak temperature. The amount of precipitation of $Cr_2N$ at the grain boundary and in the grain increased with increasing peak temperature. The region around $Cr_2N$ showed intergranular corrosion.*

*For the sensitization at 923K for 72ks, σphase precipitated and secondary γphases (named γ*phase) appeared between primary γphase and σphase. The γ* phases were predominantly corroded and the pitting potentials were low.*

*Stress corrosion cracking in high temperature water hardly occurred for the solution-treated specimen. The reduction in area of the specimen sensitized at 923K for 72ks was much lower than that of the solution-treated specimens and decreased with decreasing peak temperature, because the γ* phases near the $M_{23}C_6$ and σphase were predominantly corroded and dissolved.*

**KEY WORDS:** (Secondary Austenite),(Corrosion),(Stress Corrosion Cracking), (Sensitization), (Weldment),(Duplex Stainless Steel)

## 1. Introduction

In boiling water reactor (BWR) environments, intergranular stress corrosion cracking has occurred at the weld heat affected zone (HAZ) of austenitic stainless steels. The cause is generally known to correlate with sensitization, residual stress and dissolved oxygen[1)-4)].

Duplex stainless steels having a two phase ferritic-austenitic microstructure were compared with austenitic stainless steel and showed higher mechanical strengths, superior resistance to corrosion and stress corrosion cracking[5)-7)]. The duplex stainless steels are used extensively in the nuclear, oil, and chemical industries.

In nuclear reactors designed to operate for 40 years at 550-573K, it is difficult to evaluate the microstructure change for the long aging time. The current "best estimates" of the degree of embrittlement at the reactor operating temperature are obtained from Arrhenius extrapolations of the laboratory data obtained at higher temperatures such as 673K[8)].

In case of austenitic stainless steel, the sensitization causes intergranular stress corrosion cracking in high temperature water[1),2)]. The sensitization means that a Cr depleted zone occurs owing to the $M_{23}C_6$ precipitation at the grain boundary and leads to intergranular corrosion by the heating at 923K[1),9)].

In case of the duplex stainless steel, secondary austenite, σ phase and $M_{23}C_6$ will occur by the sensitization[10,11)]. But the relation between microstructure in the HAZ, and corrosion and stress corrosion cracking in high temperature water has not yet been clarified, when the weldment has suffered sensitization.

† Received on December 20, 1994
* Assistant Professor
** Professor

Transactions of JWRI is published by Welding Research Institute, Osaka University, Ibaraki, Osaka 567, Japan

The effect of secondary austenite on corrosion and stress corrosion cracking in high temperature water for sensitized duplex stainless steel weldments was investigated using transmission electron microscopy and fractography.

## 2. Experimental Procedure

The material used in this study is SUS329J1 steel and the chemical composition is shown in **Table 1**. The plain tensile specimen for the stress corrosion cracking test in an autoclave was 4mm diameter and 20mm long.

It is difficult to extract the tensile specimen from the narrow HAZ. So, in this investigation, the microstructure in the HAZ was simulated by a heat treatment on the basis of the weld thermal cycle.

The samples were heated at various peak temperatures for 1.8ks, water-quenched and then sensitized at 923K for 72ks. The microstructure was observed by means of transmission electron microscopy using thin foils. The identification of the precipitates and phases in the samples was accomplished by X-ray diffraction techniques and selected area electron diffraction techniques.

10% oxalic acid tests (ASTM A262A), Strauss tests (ASTM A262E) and Huey tests (ASTM A262C) were carried out for the intergranular corrosion test. For the pitting corrosion characteristics, the anodic polarization curve in 3.5% NaCl solution deaerated by bubbling argon was measured and the pitting potential was evaluated.

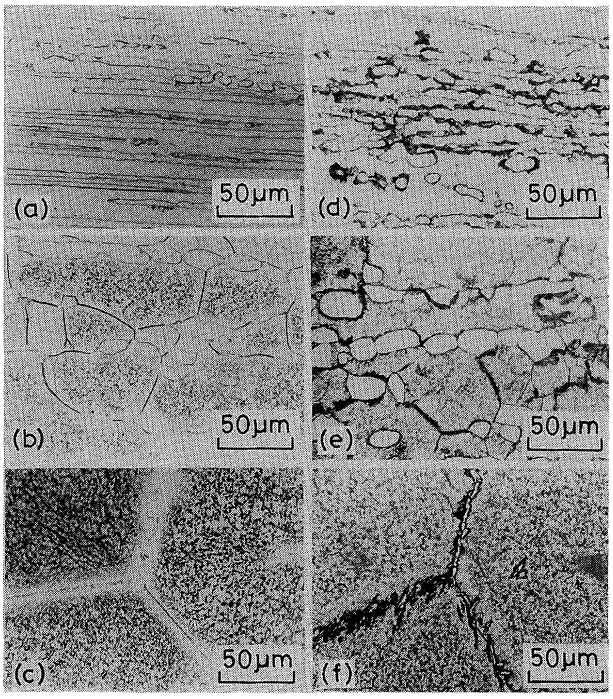


**Fig.1** Microstructures of the samples solution-treated and sensitized. (a):1273K, (b):1473K, (c):1573K, (d):1273K+923K, (e):1473K+923K, (f):1573K+923K

**Table 1** Chemical composition of duplex stainless steel (mass%).

| Material | C | Si | Mn | P | S | Ni | Cr | Mo | N |
|---|---|---|---|---|---|---|---|---|---|
| SUS329J1 | 0.014 | 0.52 | 0.31 | 0.030 | 0.006 | 4.64 | 24.92 | 1.81 | 0.14 |

The stress corrosion cracking test was performed in high temperature water at 562K with oxygen content from 0.1 ppm to 8 ppm and under 8MPa using slow strain rate testing (SSRT) at $4.17 \times 10^{-6} s^{-1}$. The dissolved oxygen was automatically controlled by introducing nitrogen gas and oxygen gas.

The susceptibility to stress corrosion cracking was evaluated by the rupture strain and reduction in area. The fracture surface after the stress corrosion cracking test was observed in detail using a scanning electron microscope.

## 3. Results and Discussion

### 3.1 Effect of microstructure on corrosion

**Figure 1** indicates the microstructures of the samples heated at various temperatures (a)-(c) and then sensitized (d)-(f). The elongated γ phases are present in the α matrix up to 1273K. For the sample heated at 1473K, the γ phase is coarse-grained, and $Cr_2N$ precipitates at the α grain boundaries and fine $Cr_2N$ precipitates in the α grain are observed.

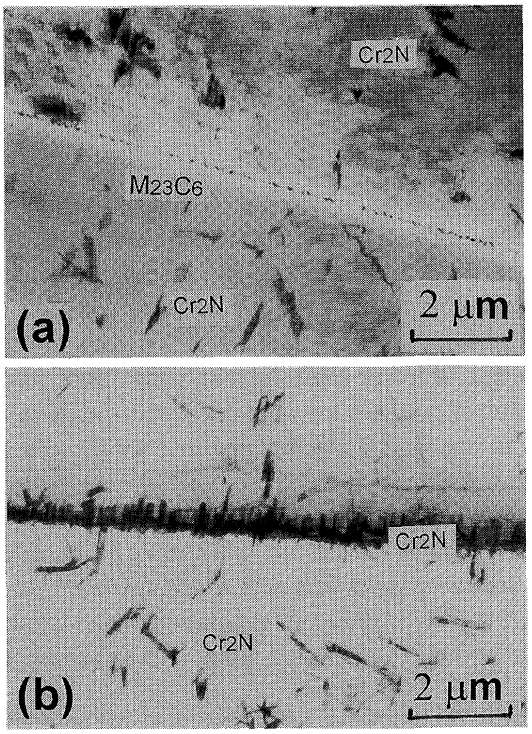


**Fig.2** Transmission electron micrographs of the samples solution-treated at 1473K.

For the sample heated at 1573K, γ phase precipitates at the grain boundary and many fine $Cr_2N$ precipitates are present in the grain. The α phase increased with increasing peak temperature, and volume fracion of γ phase decreased with increasing peak temperature and the grain size of the γ phase increased with increasing peak temperature. The amount of precipitated $Cr_2N$ at the grain boundary and in the grain increased with increasing peak temperature.

In the case of sensitized samples, many darkened coarse precipitates are present in the α/γ interface for the sample heated at 1273K. For the sample heated at 1473K, some γ phase precipitated at the α grain boundary and α/γ interface. Transmission electron microscopy was carried out to examine the precipitates in detail.

**Figure 2** shows transmission electron micrographs of the specimens solution-treated at 1473K. $M_{23}C_6$ and $Cr_2N$ are observed at α/α interface shown in Figs.2-(a) and (b) respectively. Fine $Cr_2N$ is also observed within the α grain. In case of the as-received specimen and the specimen solution-treated at 1273K, no precipitates are observed. Consequently, the precipitates in the α grain shown in Figs. 1-(b) and (c) are $Cr_2N$. The as-received material used in this study contains 1400ppm of nitrogen and the volume fraction of γ phase is 38%.

The volume fraction of the γ phase decreases with increasing peak temperature.

Consequently, nitrogen dissolved in the γ phase is swept out of the γ phase into the α phase. Nitrogen precipitates as $Cr_2N$ in the α phase and at α/α interfaces, because the solubility of nitrogen in the α phase is very low.

**Figure 3** shows transmission electron micrographs of the as-received sample which was sensitized at 923K. Darkened σ phases are observed around the γ phases as shown in Fig.3-(a). For more detail observation, as shown in Fig.3-(b), secondary γ phase (named γ* phase) appeared between primary γ phase and σ phase.

The γ* phase was more thinned than the primary γ phase after the electrolytical thinning treatment. This suggests that the chemical composition of the γ* phase is different from that of the primary γ phase. Chromium and molybdenum in the γ* phase seem to be less than that of the primary γ phase. $M_{23}C_6$ also precipitated between the γ* phase and the primary γ phase.

Aging sequence indicates that the precipitation of $M_{23}C_6$ first, the precipitation of γ* phase next and then the precipitation of σ phase occurred. The precipitation at the α/γ* boundary of σ phase occurred at a later stage.

**Figure 4** shows transmission electron micrographs of the specimens solution-treated at 1273K and then sensitized. $M_{23}C_6$ precipitates at α/α interfaces and the bowing of the γ phase (called γ* phase) from the primary

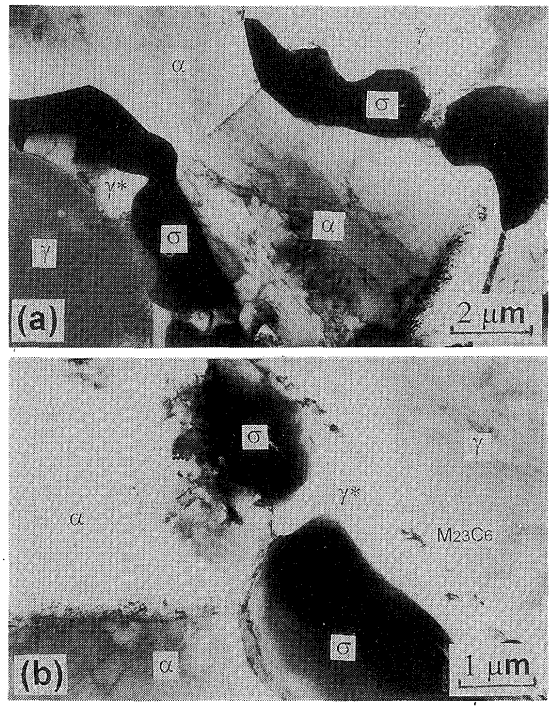


**Fig.3** Transmission electron micrographs of the as-received specimen sensitized at 923K.

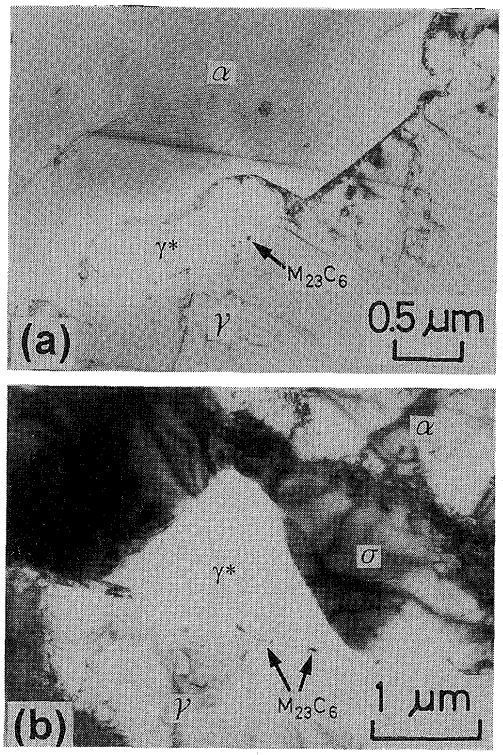


**Fig.4** Transmission electron micrographs of the specimen solution-treated at 1273K and sensitized at 923K.

γ phase to the α phase are observed as shown in Fig.4-(a). No $Cr_2N$ is observed within the α phase. Another region shows that $M_{23}C_6$, γ* phase and σ phase at the α/γ interface precipitate as shown in Fig.4-(b).

**Figure 5** indicates transmission electron micrographs of the sample heated at 1473K and then sensitized at 923K. Two kinds of microstructures are observed at α/γ interface. Fig.5-(a) indicates that $M_{23}C_6$ precipitated at the α/γ interface first and then γ* phase precipitated later, but σ phase has not precipitated yet. Fig.5-(b) indicates that $M_{23}C_6$ precipitated and then γ* phase and σ phase precipitated.

**Figure 6** indicates surface appearances after the Strauss test for the as-received specimen solution-treated (a) and sensitized (b). For the solution-treated specimen, intergranular corrosion hardly occurred.

For the sensitized specimen, the regions between σ phase and α phase are corroded, though σ phases are hardly corroded. This means that γ* phase shown in Fig.3-(b) is preferentially corroded.

Nilsson et al [5] reported using analytical transmission electron microscopy that chromium and molibdenum in the secondary γ* phase are lower than in the primary γ phase .

In this study, the specimens are sensitized at 923K for 72ks. Strauss testing causes the corrosion at regions below 13% chromium. Consequently, γ* phases are preferentially corroded and the chromium concentration of the γ* phase seems to be below 13%.

**Figure 7** indicates the effect of peak temperature on pitting potential in 3.5% NaCl solution. For the solution-treated sample, the pitting potential fairly decreases with increasing peak temperature. The pits occurred at the a/a interface in every sample.

For the sensitization, the pitting potentials of the as-received sample and the sample heated below 1373K are much lower than those of the samples heated at 1473K and 1573K. Pits generated at γ/σ interface were observed by means of optical microscopy.

Consequently, the pits are considered to have generated in the γ* phase between α phase and σ phase. The pitting potential of the samples heated at lower temperature is very low.

This suggests that the chromium concentration in the γ* phase is lower than that of the primary γ phase. Strauss tests and Huey tests were also carried out to determine which region was corroded, and they revealed that the γ* phase and the region around the σ phase were preferentially corroded.

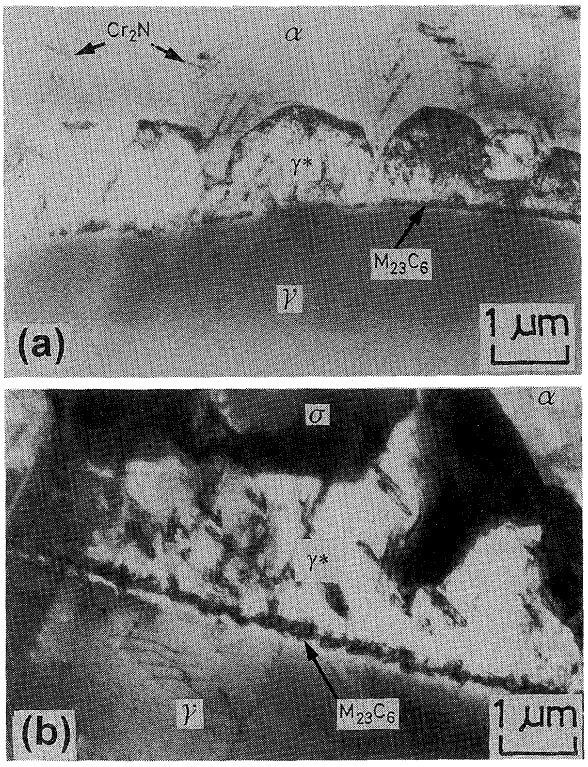


**Fig.5** Transmission electron micrographs of the specimen solution-treated at 1473K and sensitized at 923K.

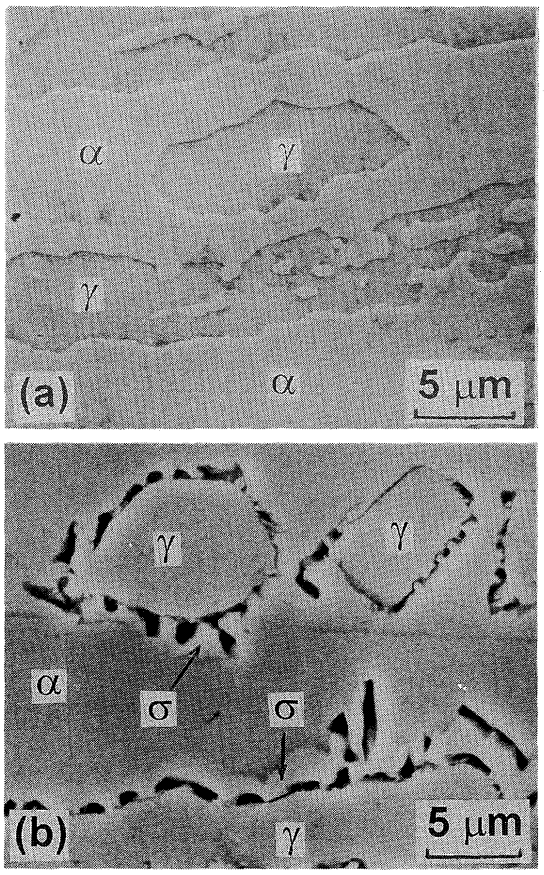


**Fig.6** Surface appearances after Strauss test for the as-received specimen.(a): Solution-treated, b):Sensitized

### 3.2 Stress corrosion cracking in high temperature water

**Figure 8** shows the effect of peak temperature on reduction of area for the specimen tested at room temperature in air. In case of the solution-treated specimen, the reductions of area are high for the as-received specimen and the specimen heated at 1273K.

The reduction of area decreases with increasing peak temperature, because of the increase of the α phase.

In case of the sensitized specimen, the reduction of area of the as-received specimen is much lower. The reduction of area increases with increasing peak temperature.

This means that the precipitaion of σ phase increases with decreasing peak temperature and the reduction of area decreases accordingly. The precipitations of σ phase are small and the decrease of reduction of area are also small.

Generally, stress corrosion cracking in high temperature water hardly occurs below 1 ppm dissolved oxygen and high strain rate for austenitic stainless steel[1]. In this section, the effect of strain rate and dissolved oxygen on the stress corrosion cracking in high temperature water was investigated.

**Figure 9** indicates the effect of testing condition on reduction of area when the as-received specimens were tested in high temperature water. In the case of high strain rate testing of $8.33 \times 10^{-4} s^{-1}$, the reduction of area is 75% at 300K, but it is 63% at 562K with 8 ppm.

The stress corrosion cracking was hardly visible on the basis of fractography which showed a dimple pattern. Serration was observed during the tensile test, the fracture indicated a 45 degree direction toward tensile axis. This means that the embrittlement by dynamic strain aging has occurred during testing at 562K.

The reduction of area for the specimen under the condition of 0.1 ppm dissolved oxygen, a strain rate of $4.17 \times 10^{-6} s^{-1}$ and at 562K shows almost same as that for the specimen under the condition of 8 ppm dissolved oxygen, $8.33 \times 10^{-4} s^{-1}$ and at 562K.

Consequently, the stress corrosion cracking in high

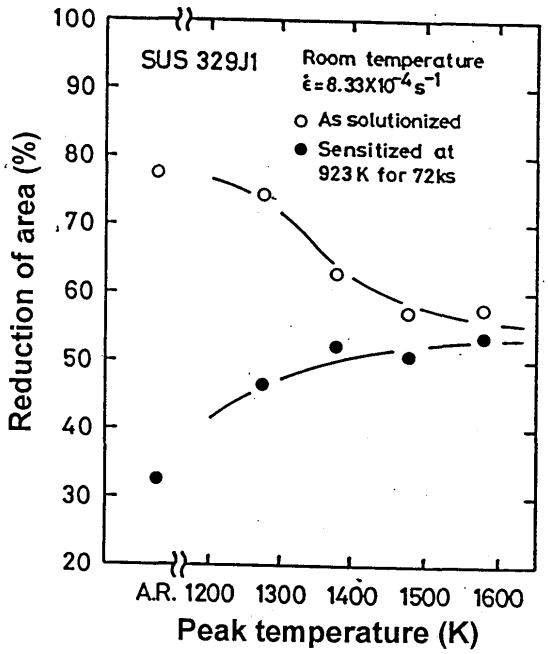


**Fig.8** Effect of peak temperature on reduction of area for the specimens tested at 300K in air.

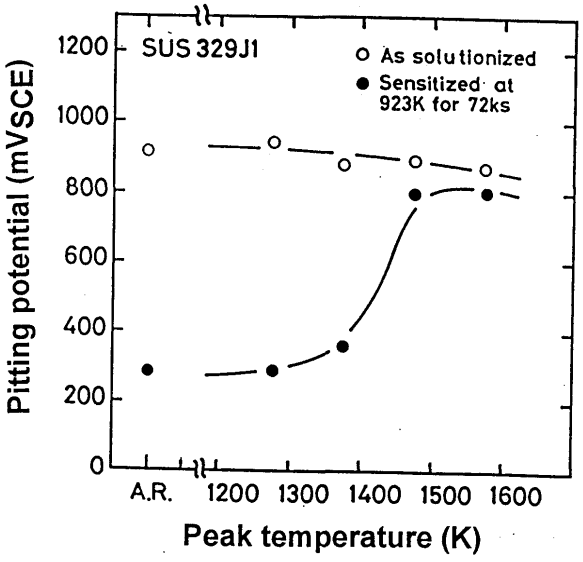


**Fig.7** Effect of peak temperature on pitting potentia in 3.5% NaCl solution for the samples solution-treated at various peak temperatures and then sensitized at 923K.

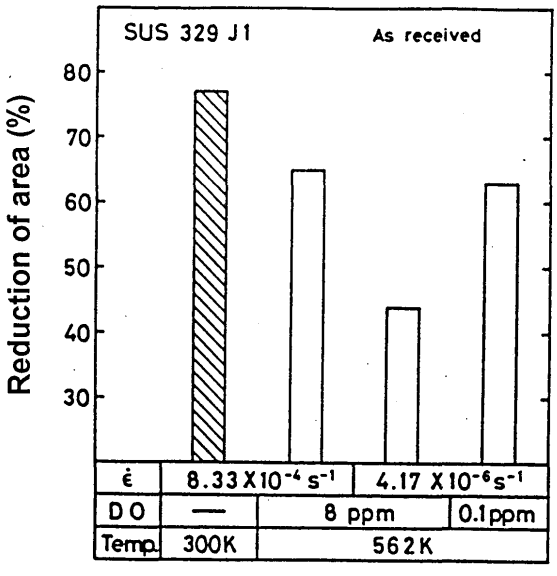


**Fig.9** Effect of test condition on reduction of area, as the as-received specimens were tested in high temperature water.

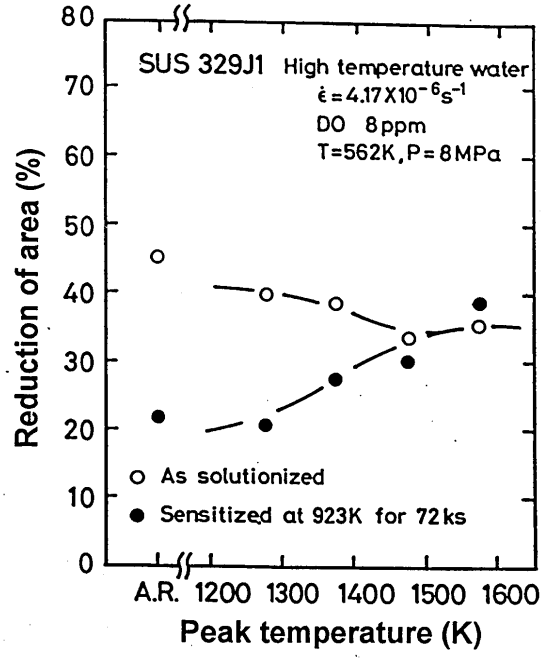


**Fig.10** Effect of peak temperature on reduction of area, as the solution-treated at various peak temperatures and then sensitized specimens were tested in high temperature water by SSRT.

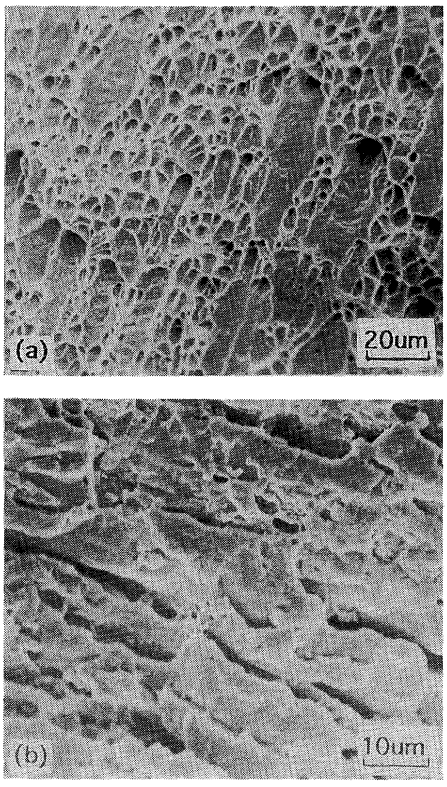


**Fig.11** Fracture morphology after SSRT in high temperature water for the as-received specimens.(a):Solution-treated, (b):Semsitized.

temperature water at 562K hardly occurs when dissolved oxygen is 0.1 ppm and low strain rate testing, such as $4.17 \times 10^{-6} s^{-1}$, is carried out. The reduction of area is 42% for the specimen at 562K tested at $4.17 \times 10^{-6} s^{-1}$ and with 8 ppm. These conditions were used for later tests.

**Figure 10** shows the effect of peak temperature on reduction of area, as the specimens were tensile-tested at 562K with 8 ppm at the strain rate of $4.17 \times 10^{-6} s^{-1}$ by means of SSRT.

In case of the solution-treated specimen, the reduction of area decreases with increasing peak temperature. Compared to the result in Fig.6, the reductions of area of the specimen tested at 562K are much lower than that of the specimen tested at room temperature.

The fracture surface showed a dimple pattern and the stress corrosion cracking in high temperature water hardly occurred. So the lowering of the reduction of area is considered to be due to the dynamic strain aging previously described.

In case of the sensitized specimen, the reductions of area are considerably lower than that of the solution-treated specimen. Stress corrosion cracking in high temperature water occurred easily when as-received specimen

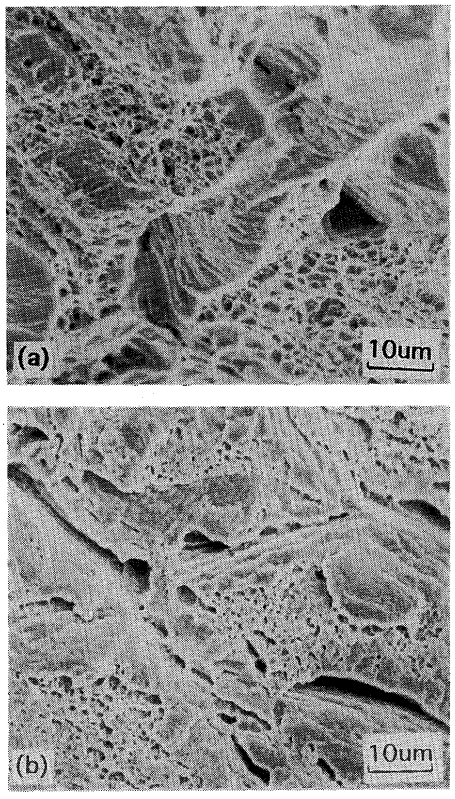


**Fig.12** Fracture morphology after SSRT in high temperature water for the specimens solution-treated at 1473K and sensitized. (a):Solution-treated, (b):Semsitized.

and the specimen heated at lower peak temperature were sensitized.

**Figure 11** shows fracture morphology after the SCC test in high temperature water for the as-received specimen. In case of solution-treated sample shown in Fig.11-(a), the fracture morphology shows a dimple pattern and a plain region owing to the decohesion at $\alpha/\gamma$ interface.

The plain region is also observed for the specimen tested at room temperature in air. However, the region in the specimen tested in high temperature water is much larger than that of the specimen tested at room temperature in air.

In case of the sensitized specimen shown in Fig.11-(b), $\alpha/\gamma$ regions including $\gamma^*$ phase, $M_{23}C_6$ and $\sigma$ phase are predominantly corroded and dissolved. The $\gamma^*$ phases are considered to be corroded preferentially, because of lower chromium concentration than that surrounding regions.

**Figure 12** indicates the fracture morphology after the SCC test in high temperature water for the specimen solution-treated at 1473K and then sensitized.

For the solution-treated specimen, the fracture morphology shows a dimple pattern as shown in Fig.12-(a). The fine dimple pattern is observed owing to the fine precipitation of $Cr_2N$ in the $\alpha$ phase. For the sensitized specimen shown in Fig.12-(b), the region of $\gamma$ phase is flat and $\alpha/\gamma$ interface are corroded predominantly.

Comparing the microstructures, it is concluded that corrosion occurs at the $\gamma^*$ phase, $\sigma$ phase causes the lowering of the mechanical strength such as reduction in area and $\gamma^*$ phases are predominantly corroded and dissolved during the SCC test in high temperature water.

## 4. Conclusion

The effect of microstructure on stress corrosion cracking in high temperature water for duplex stainless steel weldments was investigated using slow strain rate testing (SSRT), transmission electron microscopy and fracto-graphy. The results obtained in this study are summarized as follows.

(1)Volume fraction of $\gamma$ phase decreased with increasing peak temperature and the grain size of the $\gamma$ phase increased with increasing peak temperature. The amount of precipitation of $Cr_2N$ at the grain boundary and in the grain increased with increasing peak temperature. The region around $Cr_2N$ showed intergranular corrosion.

(2)For sensitization at 923K for 72ks, $\sigma$ phase precipitated and secondary $\gamma$ phases (named $\gamma^*$ phase) appeared between primary $\gamma$ phase and $\sigma$ phase. $\sigma$ phase increased with decreasing peak temperature. The $\gamma^*$ phases were predominantly corroded and the pitting potentials were low.

(3)Stress corrosion cracking in high temperature water at 562K hardly occurs when the dissolved oxygen is 0.1 ppm and the slow strain rate testing at $4.17\times10^{-6}s^{-1}$ is carried out. The stress corrosion cracking test at 562K was carried out under the condition of dissolved oxygen of 8 ppm and strain rate of $4.17\times10^{-6}s^{-1}$ for later tests, and the stress corrosion cracking in high temperature water hardly occurred for the solution-treated specimen.

The reduction in area of the specimen sensitized at 923K for 72ks was much lower than that of the solution-treated specimen and decreased with decreasing peak temperature, because the $\gamma^*$ phases near the $M_{23}C_6$ and $\sigma$ phase were predominantly corroded and dissolved during the test.

## References


1)M.Kowaka ; Corrosion Damage of Metals and Its Improvement Technology, Agunne, Tokyo, (1983)
2)T.Kuroda , Y.Kikuchi , Yen Y and T. Enjo T; Quart. J Japan Welding Soc., 8-3, (1990), 384 (in Japanese)
3)T. Kuroda, K. Okabe and T. Enjo; Quart. J. Japan Welding Soc., 8-3, (1990), 397 (in Japanese)
4)T. Kuroda, Y. Yen and T. Enjo; Quart. J. Japan Welding Soc., 8-3, (1990), 391 (in Japanese)
5)J.O. Nilsson; Mater. Sci. and Tech., 8-8, (1992), 685
6)T. Kuroda, K. Bunno and T. Enjo; J. Mater. Sci. of Japan, 40-453, (1991), 730 (in Japanese)
7)T. Enjo, T. Kuroda and K. Imanishi; J. Mater. Sci. of Japan, 38-428, (1989), 472 (in Japanese)
8)K. Chopra and H.M. Chung; Proc. Int. Symp. Environmental Degradation of Materials in Nuclear Power System Water Reactor, Aug., (1987), Traverse City, MI
9)E.L. Hall and C.L.Briant; Metall. Trans. A, 15A-5, (1984), 793
10)J.O. Nilsson and A. Wilson; Mater. Sci. and Tech., 9-7, (1993), 545
11)D.J. Kotecki; Weld. J. (1989), 431s